2020 International Conference on Unmanned Aircraft Systems (ICUAS)
Athens, Greece. September 1-4, 2020

Modeling and Control of a Novel Over-actuated Tri-rotor UAV*

Yunhe Wang, Zhangzhen Zhu, and Yu Zhang

Abstract— **This paper presents a novel tilting tri-rotor unmanned aerial vehicle (UAV) based on the conventional tri-rotor configuration, with each rotor having two tilting degrees of freedom, which is an over-actuated system. Herein, the dynamic model of this novel UAV is developed, which has nine controllable variables. Owing to the nonlinear and coupled nature of the system, many conventional nonlinear control allocation algorithms are too computationally complex to be calculated online. Therefore, a new control allocation method is proposed by using a reversible mapping to transform the nonlinear control allocation problem to the corresponding linear control allocation problem. The feedback linearization method is used to implement the entire control architecture using the new control allocation algorithm. Furthermore, a nonlinear disturbance observer (NDOB) is used to combat the low robustness of the feedback linearization controller. Finally, several simulation experiments are conducted to validate the proposed method. The simulations reveal that the fuselage can successfully track different spatial trajectories with different attitudes, which corroborates the high maneuverability of the fuselage over the conventional quadrotor.**

I. INTRODUCTION

In recent decades, unmanned aerial vehicles (UAVs) have attracted increasing research attention owing to their wide applications and significant potential [1]. UAVs come in a wide variety of shapes and sizes and have many advantages over manned aircrafts. The studies on UAVs mainly focus on their structure and control method. With regard to the control method, many control algorithms have been successfully implemented on UAVs. A classical cascade proportional–integral–derivative (PID) algorithm has been implemented in a quadrotor [2], [3]. The active disturbance rejection control (ADRC) method has been implemented in a fixed-wing UAV [4] and quadrotor [5]. Moreover, the H-infinity control method, adaptive method, and model predictive control method have also been introduced for controlling a nonlinear UAV model [6], a linear UAV model [7] and a multirotor [8], respectively. With regard to the structure, UAVs can be broadly classified into rotorcrafts, fixed-wing UAVs, and numerous other novel UAVs. Rotorcrafts have many unique properties, such as vertical take-off and landing (VTOL) and hovering; however, they exhibit some problems such as poor endurance [9]. Fixed-wing UAVs have high endurance, owing to their flight mechanics, but lack VTOL capability. Meanwhile, numerous novel UAVs have been proposed to accomplish various tasks. For instance, hybrid UAVs are an attempt to combine the advantages of rotorcrafts and fixed-wing UAVs; they can switch between two different flight modes depending on the task [10], [11], [12], [13]. Furthermore, numerous nonconventional UAVs have been proposed; for example, [14], [15], [16] and the literature therein [17].

Among these nonconventional UAVs, thrust vectoring is a research hotspot in the field of UAV structure research. In fact, many researchers have introduced this concept to rotorcraft design to enhance the mobility and agility of rotorcrafts by giving rotors one or more tilting DOFs, which means that the rotor thrust vector can tilt in space, thereby enhancing the maneuverability of the body [18], [19], [20], [21]. However, many rotorcrafts, such as the UAV model this study proposes, may become over-actuated systems instead of underactuated systems because of the given tilting DOFs. The over-actuated system has more control inputs than control outputs, which means that the controller for the over-actuated system can be designed with more freedom and more challenges. Control allocation is a prevalent way of tackling over-actuated systems, and it also has the ability of tolerating the faults of the actuators. Specifically, the control allocation process maps a virtual control signal generated from the control loop into actuator commands that provide actual control efforts. Owing to the redundancy in actuators, the mapping from the virtual control to actuator commands is a one-to-many mapping [22].

We suppose the system can be described as

$$\begin{cases} \dot{\boldsymbol{x}} = f(\boldsymbol{x}, t) + g(\boldsymbol{x}, t)\,\boldsymbol{U} \\ \boldsymbol{y} = l(\boldsymbol{x}, t) \end{cases} \tag{1}$$

where $\boldsymbol{U}$ is the control input. The basic problem statement of control allocation is expressed as follows:

$$\begin{aligned} &\min_{\boldsymbol{\tau}} J(\boldsymbol{x}, \boldsymbol{\tau}, t) \qquad s.t. \quad \boldsymbol{U} = h(\boldsymbol{x}, \boldsymbol{\tau}, t) \\ &\Omega_1 = \left\{ \tau_i \in \mathbb{R}^m | \tau_{\min} \leqslant \tau_i \leqslant \tau_{\max} \right\} \\ &\Omega_2 = \left\{ \dot{\tau}_i \in \mathbb{R}^m | \rho_{\min} \leqslant \dot{\tau}_i \leqslant \rho_{\max} \right\}. \end{aligned}$$

The $\tau_{\min}$, $\tau_{\max}$, $\rho_{\min}$, and $\rho_{\max}$ are the limits of the actuator variable $\boldsymbol{\tau}$, and $J(\boldsymbol{x}, \boldsymbol{\tau}, t)$ is the cost function. In general, we can divide the control allocation problem into linear control allocation and nonlinear control allocation based on whether the equation $h(\boldsymbol{x}, \boldsymbol{\tau}, t) = B(\boldsymbol{x}, t)\,\boldsymbol{\tau}$ holds. The linear control allocation methods have been carefully organized by scholars [23]. These methods are valid and classical.

*This work was supported by the National Natural Science Foundation of China (Grant No. 61673341), National Key R&D Program of China (2016YFD0200701-3), the Project of State Key Laboratory of Industrial Control Technology (Zhejiang University) (No. ICT1913) and the Open Research Project of the State Key Laboratory of Industrial Control Technology, Zhejiang University, China (No. ICT1900312).

College of Control Science and Engineering, and State Key Laboratory of Industrial Control Technology, Zhejiang University, Hangzhou, 310027 China {21832137, 11832015, zhangyu80}@zju.edu.cn

Sometimes, the effectiveness equation is nonlinear [24] like this study, which means it is a nonlinear control allocation problem. Therefore, many researchers have presented several valid approaches, including nonlinear programming [25] and mixed-integer programming [26]. Unlike the linear control allocation case, in the nonlinear case, there is little hope of finding a general-purpose nonlinear programming algorithm and numerical software implementation for general nonlinear allocation problems [27], which means that we need to analyze each specific nonlinear problem. The effector model in this study is also nonlinear. Herein, we propose a new control allocation method to tackle the high nonlinearity of the model.

The remainder of the paper is organized as follows. The dynamic model of the UAV is presented in SectionII, and the entire control architecture is designed in SectionIII. SectionIV discusses the results of simulation experiments performed to validate the proposed approach. Simulations are implemented on some specific trajectories and the convergence results are obtained. Any divergence that may occur between the simulation and reference results is discussed. Conclusions are presented in SectionV.

II. DYNAMIC MODEL

A. Structure of the Novel UAV

Conventional rotorcrafts, such as tri-rotor and quadrotor UAVs, adjust the rotor lift by simultaneously increasing or decreasing the rotational speed of the rotors to enable movement in the vertical direction. If movement is required in the horizontal direction, the fuselage must be tilted using the component force in the horizontal direction, thereby pushing the fuselage forward. Clearly, this way of moving forward is inefficient and limited because there are fewer controllable variables than motion DOFs in the conventional model (underactuated system). In this study, each pair of coaxial rotors in the conventional tri-rotor have tilting degrees in two directions, which means an over-actuated system. Compared with the fully-actuated system, the actuators' status of the over-actuated system are not unique, which means a cost function can be set to optimize the flight task. The specific model structure is shown in Fig.1.

Including the rotation speed of the six rotors that can be controlled, there are 12 controllable variables in the entire model. Therefore, in order to simplify the problem, the speed of the coaxial rotors is made equal, resulting in nine controllable variables after simplification. For the aircraft to move in the vertical direction, only three rotors are required. If horizontal flight is required, the rotors can be tilted in the desired direction, without needing to first tilt the fuselage. When more complex curved motion is required, the superiority of the proposed model over the underactuated model is dramatic.

B. Description of the Dynamic Model

Before discussing the specific equations of motion, the coordinate system used in this study is defined and illustrated.

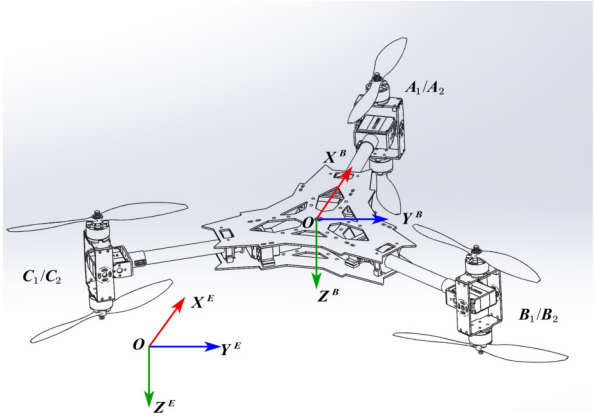

Fig. 1: Structure of the novel tilting tri-rotor system

The ground coordinate system $Ox^Ey^Ez^E$ and the body coordinate system $Ox^By^Bz^B$ are both established as shown in Fig.1. We arbitrarily select a point on the surface of the Earth as the coordinate origin O, the direction of Ox^E points is parallel with the ground, the direction of Oz^E points is vertically downward, and the direction of Oy^E is determined by the right-hand coordinate law. Here, our model does not consider the influence of the Earth's rotation; thus, the ground coordinate system is an inertial coordinate system.

Furthermore, in order to analyze the core problem and ignore the various subordinate factors, we employ the following assumptions:

Assumption 1: The fuselage is a rigid body.

Assumption 2: The effects of air resistance and wind are not considered. Concrete models of air resistance and wind are hard to obtain; thus, we specifically implement lumped disturbance items in SectionIII where we discuss the disturbance observer in detail.

Assumption 3: The origin of the body coordinate system coincides with the centroid of the fuselage and the moment of inertia tensor is a diagonal matrix.

Assumption 4: The gyro effect is not considered because the rotation motion equations will be more complex if the gyro moment items are included in the equations. Furthermore, the fuselage mass and inertia moment are relatively small.

Assumption 5: To ensure that the tilting rotors do not hit the shafts, we limit the tilt angles. Thus, the tilting angles range from: $\alpha_i \in [\alpha_{min}, \alpha_{max}], \beta_i \in [\beta_{min}, \beta_{max}]$. These angles are defined in the nomenclature and depicted precisely in Fig.2. The specific values of $\alpha_{min}, \alpha_{max}, \beta_{min}$, and β_{max} are given in SectionIV.

Based on these assumptions, classical mechanics theory can be employed. According to the Newton-Euler formalism of rigid body and mechanics theories, we obtain the following formula [28]:

$$\begin{bmatrix} mI_{3\times3} & O_{3\times3} \\ O_{3\times3} & I \end{bmatrix} \begin{bmatrix} \dot{V}^B \\ \dot{\omega}^B \end{bmatrix} + \begin{bmatrix} \omega^B \times (mV^B) \\ \omega^B \times (I\omega^B) \end{bmatrix} = \begin{bmatrix} F^B \\ M^B \end{bmatrix} \tag{2}$$

where m, $I = diag(I_x, I_y, I_z)$, $\omega^B = [p, q, r]^T$, and

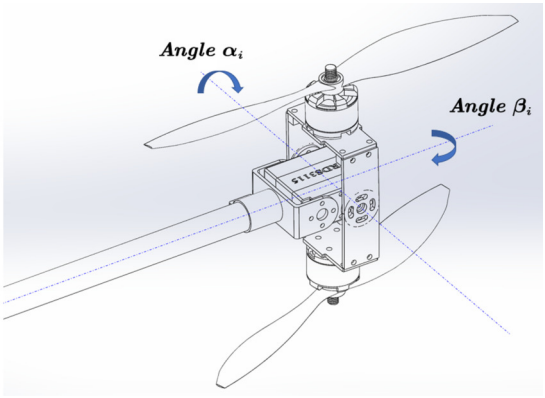

Fig. 2: Illustration of tilting angles α_i and β_i

$V^B = [u, v, w]^T$ are the mass, the second-order moment of inertia tensor, the angular velocity and velocity in the body coordinate system of the fuselage, respectively. Meanwhile, $F^B = [X_F, Y_F, Z_F]^T$ and $M^B = [L, M, N]^T$ are the external force and external torque in the body coordinate system, respectively. Equation (2) can be expanded as follows:

$$\begin{cases} \dot{u} = -g^{'} \sin\theta + rv - qw + \dfrac{X_F}{m} \\ \dot{v} = g^{'} \cos\theta \sin\phi - ru + pw + \dfrac{Y_F}{m} \\ \dot{w} = g^{'} \cos\theta \cos\phi + qu - pv + \dfrac{Z_F}{m} \end{cases} \tag{3}$$

$$\begin{cases} \dot{p} = \dfrac{I_y - I_z}{I_x} qr + \dfrac{L}{I_x} \\ \dot{q} = \dfrac{I_z - I_x}{I_y} rp + \dfrac{M}{I_y} \\ \dot{r} = \dfrac{I_x - I_y}{I_z} pq + \dfrac{N}{I_z} \end{cases} \tag{4}$$

where ϕ, θ, ψ are the roll, pitch, and yaw Euler angles of the fuselage, respectively, $g^{'}$ is the gravitational acceleration. Meanwhile, based on the coaxial structure of the fuselage and force analysis, X_F, Y_F, Z_F and L, M, N are given by:

$$\begin{bmatrix} X_F & Y_F & Z_F \end{bmatrix}^T = \begin{bmatrix} c\beta_1 s\alpha_1 & -\frac{\sqrt{3}}{2} s\beta_2 - \frac{1}{2} c\beta_2 s\alpha_2 & \frac{\sqrt{3}}{2} s\beta_3 - \frac{1}{2} c\beta_3 s\alpha_3 \\ s\beta_1 & -\frac{1}{2} s\beta_2 + \frac{\sqrt{3}}{2} c\beta_2 s\alpha_2 & -\frac{1}{2} s\beta_3 - \frac{\sqrt{3}}{2} c\beta_3 s\alpha_3 \\ -c\beta_1 c\alpha_1 & -c\beta_2 c\alpha_2 & -c\beta_3 c\alpha_3 \end{bmatrix} \begin{bmatrix} F_1 \\ F_2 \\ F_3 \end{bmatrix} \tag{5}$$

$$\begin{bmatrix} L & M & N \end{bmatrix}^T = \begin{bmatrix} 0 & -\frac{\sqrt{3}}{2} l \cos\alpha_2 \cos\beta_2 & \frac{\sqrt{3}}{2} l \cos\alpha_3 \cos\beta_3 \\ l \cos\alpha_1 \cos\beta_1 & -\frac{1}{2} l \cos\alpha_2 \cos\beta_2 & -\frac{1}{2} l \cos\alpha_3 \cos\beta_3 \\ l \sin\beta_1 & l \sin\beta_2 & l \sin\beta_3 \end{bmatrix} \begin{bmatrix} F_1 \\ F_2 \\ F_3 \end{bmatrix} \tag{6}$$

where F_1, F_2, F_3 are the sum of rotor lift for (A_1/A_2), (B_1/B_2), and (C_1/C_2), respectively, $\alpha_i, \beta_i (i = 1, 2, 3)$ are tilting angles for each pair of rotors. Here 's' means 'sin', 'c' means 'cos', the same applies below. l is the distance from rotor to centroid. Furthermore, according to [28], the conversion relationship between $[p, q, r]$ and $\left[\dot{\phi}, \dot{\theta}, \dot{\psi}\right]$, $[u, v, w]$ and $[\dot{x}, \dot{y}, \dot{z}]$ can be obtained as follows:

$$\begin{bmatrix} \dot{\phi} \\ \dot{\theta} \\ \dot{\psi} \end{bmatrix} = \begin{bmatrix} 1 & \sin\phi \tan\theta & \cos\phi \tan\theta \\ 0 & \cos\phi & -\sin\phi \\ 0 & \dfrac{\sin\phi}{\cos\theta} & \dfrac{\cos\phi}{\cos\theta} \end{bmatrix} \begin{bmatrix} p \\ q \\ r \end{bmatrix} \tag{7}$$

$$\begin{bmatrix} \dot{x} \\ \dot{y} \\ \dot{z} \end{bmatrix} = \begin{bmatrix} c\theta c\psi & c\psi s\theta s\phi - c\phi s\psi & s\phi s\psi + s\theta c\phi c\psi \\ c\theta s\psi & s\psi s\theta s\phi + c\phi c\psi & s\theta c\phi s\psi - s\phi c\psi \\ -s\theta & s\phi c\theta & c\phi c\theta \end{bmatrix} \begin{bmatrix} u \\ v \\ w \end{bmatrix} \tag{8}$$

where $[x, y, z]^T$ is the position of the fuselage centroid in the world coordinate system.

III. CONTROLLER DESIGN

The proposed system is over-actuated, and control allocation is the primary method for dealing with a nonlinear redundant system. This study employs a new control allocation algorithm to design the control framework. Meanwhile, the control law involves the multiple inputs-multiple outputs (MIMO) feedback linearization algorithm. The relative degrees of the system are equal to the number of its state vectors; therefore, this affine nonlinear system can be precisely and completely linearized by the MIMO feedback linearization method instead of approximate linearization using the Jacobian method. Furthermore, a NDOB is used to improve the robustness of the entire system. The proposed over-actuated system control architecture is illustrated in Fig.3.

A. Control Law

First, based on the discussion in SectionII, the model equation is written as a formal form of an affine nonlinear system, as follows:

$$\dot{\boldsymbol{x}} = f(\boldsymbol{x}) + g(\boldsymbol{x}) \boldsymbol{U} \tag{9}$$

$$\boldsymbol{y} = l(\boldsymbol{x}) \tag{10}$$

where $\boldsymbol{x} = [x, y, z, \phi, \theta, \psi, u, v, w, p, q, r]^T = [x_1, \cdots, x_{12}]^T$, $\boldsymbol{U} = [X_F, Y_F, Z_F, L, M, N]^T = [U_1, U_2, \cdots, U_6]^T$

$$f(\boldsymbol{x}) = \begin{bmatrix} x_7 c x_5 c x_6 + x_8 (c x_6 s x_5 s x_4 - c x_4 s x_6) + \\ x_9 (s x_4 s x_6 + s x_5 c x_4 c x_6) \\ x_7 c x_5 s x_6 + x_8 (s x_6 s x_5 s x_4 + c x_4 c x_6) + \\ x_9 (s x_5 c x_4 s x_6 - s x_4 c x_6) \\ -x_7 s x_5 + x_8 s x_4 c x_5 + x_9 c x_4 c x_5 \\ x_{10} + x_{11} s x_4 \tan x_5 + x_{12} c x_4 \tan x_5 \\ x_{11} c x_4 - x_{12} s x_4 \\ x_{11} s x_4 \sec x_5 + x_{12} c x_4 \sec x_5 \\ -g^{'} s x_5 + x_{12} x_8 - x_{11} x_9 \\ g^{'} c x_5 s x_4 - x_{12} x_7 + x_{10} x_9 \\ g^{'} c x_5 c x_4 + x_{11} x_7 - x_{10} x_8 \\ (I_y - I_z) I_x^{-1} x_{11} x_{12} \\ (I_z - I_x) I_y^{-1} x_{10} x_{12} \\ (I_x - I_y) I_z^{-1} x_{10} x_{11} \end{bmatrix} \tag{11}$$

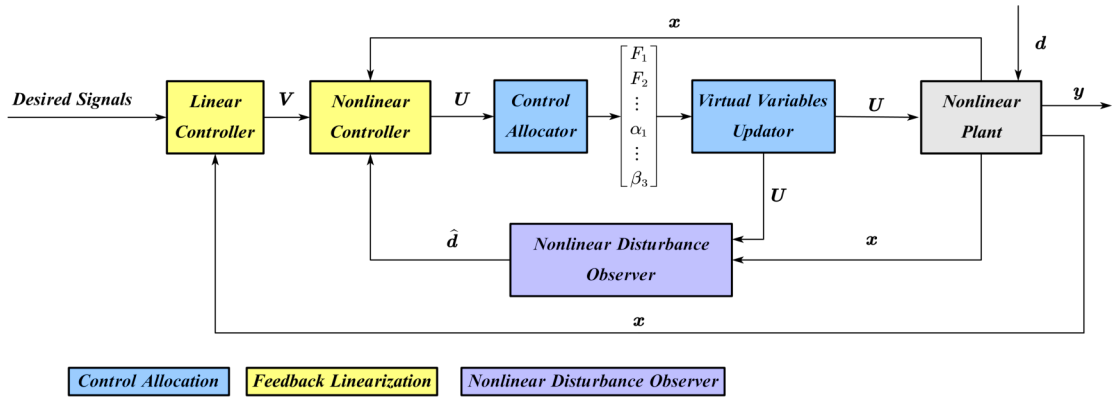

Fig. 3: Control architecture of the proposed over-actuated system

$$g(\boldsymbol{x}) = \begin{bmatrix} O_{6\times 6} \\ \operatorname{diag}\left(m^{-1}, m^{-1}, m^{-1}, I_x^{-1}, I_y^{-1}, I_z^{-1}\right) \end{bmatrix} = \left[g_1(\boldsymbol{x}), g_2(\boldsymbol{x}), \cdots, g_6(\boldsymbol{x})\right] \tag{12}$$

with

$$\boldsymbol{y} = l(\boldsymbol{x}) = [x, y, z, \phi, \theta, \psi]^T = \left[h_1(\boldsymbol{x}), h_2(\boldsymbol{x}), \cdots, h_6(\boldsymbol{x})\right]^T. \tag{13}$$

According to the theory of feedback linearization of the MIMO system [29], it is necessary to first determine the total relative degree of the system.

We have,

$$\mathscr{L}_{g_j} h_i(x) = \frac{\partial h_i(\boldsymbol{x})}{\partial \boldsymbol{x}^T} g_j(\boldsymbol{x}) = 0, \quad 1 \leqslant i, j \leqslant 6. \tag{14}$$

Meanwhile, $\mathscr{L}_{g_j}\mathscr{L}_f h_i(x) = \mathscr{L}_{g_j}\dfrac{\partial h_i(\boldsymbol{x})}{\partial \boldsymbol{x}^T} f(\boldsymbol{x}) = \dfrac{\partial}{\partial \boldsymbol{x}^T}\left(\dfrac{\partial h_i(\boldsymbol{x})}{\partial \boldsymbol{x}^T} f(\boldsymbol{x})\right) g_j(\boldsymbol{x})$, $1 \leqslant i, j \leqslant 6$ and the decoupling matrix $\Gamma(\boldsymbol{x})$ is obtained as follows:

$$\Gamma(\boldsymbol{x}) = \begin{bmatrix} \mathscr{L}_{g_1}\mathscr{L}_f h_1(\boldsymbol{x}) & \cdots & \mathscr{L}_{g_6}\mathscr{L}_f h_1(\boldsymbol{x}) \\ \mathscr{L}_{g_1}\mathscr{L}_f h_2(\boldsymbol{x}) & \cdots & \mathscr{L}_{g_6}\mathscr{L}_f h_2(\boldsymbol{x}) \\ \vdots & & \vdots \\ \mathscr{L}_{g_1}\mathscr{L}_f h_6(\boldsymbol{x}) & \cdots & \mathscr{L}_{g_6}\mathscr{L}_f h_6(\boldsymbol{x}) \end{bmatrix} = \begin{bmatrix} K_1 & O_{3\times 3} \\ O_{3\times 3} & K_2 \end{bmatrix} \tag{15}$$

where

$$K_1 = \frac{1}{m}\begin{bmatrix} cx_5cx_6 & cx_6sx_5sx_4 - cx_4sx_6 & sx_4sx_6 + sx_5cx_4cx_6 \\ cx_5sx_6 & sx_6sx_5sx_4 + cx_4cx_6 & sx_5cx_4sx_6 - sx_4cx_6 \\ -sx_5 & sx_4cx_5 & cx_4cx_5 \end{bmatrix} \tag{16}$$

$$K_2 = \begin{bmatrix} I_x^{-1} & I_x^{-1}\sin x_4 \tan x_5 & I_x^{-1}\cos x_4 \tan x_5 \\ 0 & I_y^{-1}\cos x_4 & -I_y^{-1}\sin x_4 \\ 0 & I_z^{-1}\dfrac{\sin x_4}{\cos x_5} & I_z^{-1}\dfrac{\cos x_4}{\cos x_5} \end{bmatrix}. \tag{17}$$

The matrix mK_1 is orthogonal, so we know $|mK_1| = 1$, which means that $|\Gamma(\boldsymbol{x})| = |K_1||K_2| = (mI_xI_yI_z\cos x_5)^{-1}$. Therefore, $|\Gamma(\boldsymbol{x})| \neq 0$ and the matrix $\Gamma(\boldsymbol{x})$ is nonsingular and invertible when $\cos x_5 \neq 0 \Leftrightarrow x_5 = \theta \neq \delta\pi + \dfrac{\pi}{2}$ $(\delta \in \mathbb{Z})$, which means the relative degree vector of the system is obtained:

$$r_i = 2, \quad (1 \leqslant i \leqslant 6). \tag{18}$$

The total relative degree is

$$r_0 = \sum_{i=1}^{6} r_i = 2 \times 6 = 12 = n. \tag{19}$$

Meanwhile, three necessary conditions, including involutive condition and dimension of distribution condition are all met and verified. Thus, there are no internal dynamics and the entire system can be completely linearized with the control law

$$\boldsymbol{U} = \Gamma(\boldsymbol{x})^{-1}\left(-b(\boldsymbol{x}) + \boldsymbol{V}\right) \tag{20}$$

and the diffeomorphism $\boldsymbol{z} = T(\boldsymbol{x})$, where $b(\boldsymbol{x})$ is an offset item of the control law and $\boldsymbol{z} = T(\boldsymbol{x})$ is the state vector of the linearized system.

Based on the feedback linearization theory and [29], we have the following:

$$\begin{aligned} \boldsymbol{z} = T(\boldsymbol{x}) &= \left[h_1(\boldsymbol{x}) \;\; L_f h_1(\boldsymbol{x}) \cdots \;\; h_6(\boldsymbol{x}) \;\; L_f h_6(\boldsymbol{x})\right]^T \\ &= \left[x, \dot{x}, y, \dot{y}, z, \dot{z}, \phi, \dot{\phi}, \theta, \dot{\theta}, \psi, \dot{\psi}\right]^T \\ b(\boldsymbol{x}) &= \left[L_f^2 h_1(\boldsymbol{x}) \;\; L_f^2 h_2(\boldsymbol{x}) \;\; \cdots \;\; L_f^2 h_6(\boldsymbol{x})\right]^T \\ &= \left[\frac{\partial f_1}{\partial \boldsymbol{x}}, \frac{\partial f_2}{\partial \boldsymbol{x}}, \frac{\partial f_3}{\partial \boldsymbol{x}}, \frac{\partial f_4}{\partial \boldsymbol{x}}, \frac{\partial f_5}{\partial \boldsymbol{x}}, \frac{\partial f_6}{\partial \boldsymbol{x}}\right]^T \end{aligned}$$

where f_i represents the i-th component of f. According to (10) $\sim$ (21), Equation (10) can be linearized into a linear time-invariant relationship, as follows:

$$\begin{cases} \dot{\boldsymbol{z}} = A_0\boldsymbol{z} + B_0\boldsymbol{V} \\ \boldsymbol{\xi} = C_0\boldsymbol{z} \end{cases} \tag{21}$$

where $A_0 = \operatorname{diag}(\Delta_1, \cdots, \Delta_1)$, $B_0 = \operatorname{diag}(\Delta_2, \cdots, \Delta_2)$, $C_0 = \operatorname{diag}(\Delta_3, \cdots, \Delta_3)$ and

$$\Delta_1 = \begin{bmatrix} 0 & 1 \\ 0 & 0 \end{bmatrix} \quad \Delta_2 = \begin{bmatrix} 0 \\ 1 \end{bmatrix} \quad \Delta_3 = \begin{bmatrix} 1 & 0 \end{bmatrix}$$

As the tracking control problem, we choose the control law

for the derived linear relationship ((21)):

$$V_i = \ddot{y}_{id} - \sigma_{i1}\left(\dot{y}_i - \dot{y}_{id}\right) - \sigma_{i2}\left(y_i - y_{id}\right) \ (i = 1, \cdots, 6). \tag{22}$$

The y_i and the derivative of y_i can be obtained from dynamic equation (10) in the last control cycle. The y_{id} is the desired target of the i-th component of $\boldsymbol{y}$ or $\boldsymbol{\xi}$. According to Hurwitz's theorem, if $\sigma_{i1} > 0$, $\sigma_{i2} > 0$, then all states will be asymptotically stable and the tracking error will converge to zero exponentially.

B. Control Allocation

In this study, the control effectiveness equation is described as follows:

$$\boldsymbol{U} = h\left(\boldsymbol{x}, \boldsymbol{\tau}, t\right) = \begin{bmatrix} F_1 s\alpha_1 c\beta_1 - \frac{\sqrt{3}}{2}F_2 s\beta_2 - \frac{1}{2}F_2 s\alpha_2 c\beta_2 + \frac{\sqrt{3}}{2}F_3 s\beta_3 - \\ \frac{1}{2}F_3 s\alpha_3 c\beta_3 \\ F_1 s\beta_1 - \frac{1}{2}F_2 s\beta_2 + \frac{\sqrt{3}}{2}F_2 s\alpha_2 c\beta_2 - \frac{1}{2}F_3 s\beta_3 - \\ \frac{\sqrt{3}}{2}F_3 s\alpha_3 c\beta_3 \\ -F_1 c\alpha_1 c\beta_1 - F_2 c\alpha_2 c\beta_2 - F_3 c\alpha_3 c\beta_3 \\ -\frac{\sqrt{3}}{2}F_2 l c\alpha_2 c\beta_2 + \frac{\sqrt{3}}{2}F_3 l c\alpha_3 c\beta_3 \\ F_1 l c\alpha_1 c\beta_1 - \frac{1}{2}F_2 l c\alpha_2 c\beta_2 - \frac{1}{2}F_3 l c\alpha_3 c\beta_3 \\ F_1 l s\beta_1 + F_2 l s\beta_2 + F_3 l s\beta_3 \end{bmatrix}. \tag{23}$$

The six virtual control commands: three components of external forces and three components of external moments are described as $\boldsymbol{U} = [U_1, U_2, U_3, U_4, U_5, U_6]^T$, which are on the left-hand side of the equation, and the actuator inputs are $\boldsymbol{\tau} = [F_1, F_2, F_3, \alpha_1, \alpha_2, \alpha_3, \beta_1, \beta_2, \beta_3]^T$, which are on the right-hand side of the equation. Equation (23) is the key method for dealing with this problem and combining it with the optimization function. Obviously, the control effectiveness equation (23) in this study is nonlinear. If an existing nonlinear programming method is used directly, the real-time calculation is difficult to be guaranteed. Therefore, a reversible mapping $\boldsymbol{C} = \Theta\left(\boldsymbol{\tau}\right)$ is proposed here to linearize the nonlinear problem where $\boldsymbol{C} = [a_0, b_0, \cdots, m_0]^T$ is an intermediate vector. Specifically, the reversible mapping is denoted as follows:

$$\begin{cases} a_0 = F_1 \cos\beta_1 \sin\alpha_1 \\ c_0 = F_2 \cos\beta_2 \sin\alpha_2 \\ e_0 = F_3 \cos\beta_3 \sin\alpha_3 \end{cases} \quad \begin{cases} f_0 = F_1 \sin\beta_1 \\ b_0 = F_2 \sin\beta_2 \\ d_0 = F_3 \sin\beta_3 \end{cases} \quad \begin{cases} g_0 = F_1 \cos\beta_1 \cos\alpha_1 \\ h_0 = F_2 \cos\beta_2 \cos\alpha_2 \\ m_0 = F_3 \cos\beta_3 \cos\alpha_3. \end{cases} \tag{24}$$

Meanwhile, the inverse mapping $\boldsymbol{\tau} = \Theta^{-1}\left(\boldsymbol{C}\right)$ is presented as follows:

$$\begin{cases} \tan\alpha_1 = \dfrac{F_1 \cos\beta_1 \sin\alpha_1}{F_1 \cos\beta_1 \cos\alpha_1} = \dfrac{a_0}{g_0} \\ \tan\alpha_2 = \dfrac{F_2 \cos\beta_2 \sin\alpha_2}{F_2 \cos\beta_2 \cos\alpha_2} = \dfrac{c_0}{h_0} \\ \tan\alpha_3 = \dfrac{F_3 \cos\beta_3 \sin\alpha_3}{F_3 \cos\beta_3 \cos\alpha_3} = \dfrac{e_0}{m_0} \end{cases} \Rightarrow \begin{cases} \alpha_1 = \arctan\dfrac{a_0}{g_0} \\ \alpha_2 = \arctan\dfrac{c_0}{h_0} \\ \alpha_3 = \arctan\dfrac{e_0}{m_0} \end{cases} \tag{25}$$

$$\begin{cases} \tan\beta_1 = \frac{F_1 \sin\beta_1 (\sin\alpha_1)}{F_1 \cos\beta_1 \sin\alpha_1} = \frac{f_0}{a_0} \sin\left(\tan^{-1}\frac{a_0}{g_0}\right) = \frac{f_0}{\sqrt{a_0^2+g_0^2}} \\ \tan\beta_2 = \frac{F_2 \sin\beta_2 (\sin\alpha_2)}{F_2 \cos\beta_2 \sin\alpha_2} = \frac{b_0}{c_0} \sin\left(\tan^{-1}\frac{c_0}{h_0}\right) = \frac{b_0}{\sqrt{c_0^2+h_0^2}} \\ \tan\beta_3 = \frac{F_3 \sin\beta_3 (\sin\alpha_3)}{F_3 \cos\beta_3 \sin\alpha_3} = \frac{d_0}{e_0} \sin\left(\tan^{-1}\frac{e_0}{m_0}\right) = \frac{d_0}{\sqrt{e_0^2+m_0^2}} \end{cases}$$
$$\Rightarrow \begin{cases} \beta_1 = \arctan\frac{f_0}{\sqrt{a_0^2+g_0^2}} \\ \beta_2 = \arctan\frac{b_0}{\sqrt{c_0^2+h_0^2}} \\ \beta_3 = \arctan\frac{d_0}{\sqrt{e_0^2+m_0^2}} \end{cases} \tag{26}$$

$$\begin{cases} F_1 = \frac{F_1 \sin\beta_1}{\sin\beta_1} = \frac{f_0}{\sin\left(\tan^{-1}\frac{f_0}{\sqrt{a_0^2+g_0^2}}\right)} = \sqrt{a_0^2+g_0^2+f_0^2} \\ F_2 = \frac{F_2 \sin\beta_2}{\sin\beta_2} = \frac{b_0}{\sin\left(\tan^{-1}\frac{b_0}{\sqrt{c_0^2+h_0^2}}\right)} = \sqrt{b_0^2+c_0^2+h_0^2} \\ F_3 = \frac{F_3 \sin\beta_3}{\sin\beta_3} = \frac{d_0}{\sin\left(\tan^{-1}\frac{d_0}{\sqrt{e_0^2+m_0^2}}\right)} = \sqrt{d_0^2+e_0^2+m_0^2} \end{cases}$$
$$\Rightarrow \begin{cases} F_1 = \sqrt{a_0^2+g_0^2+f_0^2} \\ F_2 = \sqrt{b_0^2+c_0^2+h_0^2} \\ F_3 = \sqrt{d_0^2+e_0^2+m_0^2} \end{cases}. \tag{27}$$

Equation (24) is substituted into (23), giving

$$\boldsymbol{U} = \boldsymbol{K}\boldsymbol{C} = \frac{1}{2}\begin{bmatrix} 2 & -\sqrt{3} & -1 & \sqrt{3} & -1 & 0 & 0 & 0 & 0 \\ 0 & -1 & \sqrt{3} & -1 & -\sqrt{3} & 2 & 0 & 0 & 0 \\ 0 & 0 & 0 & 0 & 0 & 0 & -2 & -2 & -2 \\ 0 & 0 & 0 & 0 & 0 & 0 & 0 & -\sqrt{3}l & \sqrt{3}l \\ 0 & 0 & 0 & 0 & 0 & 0 & 2l & -l & -l \\ 0 & 2l & 0 & 2l & 0 & 2l & 0 & 0 & 0 \end{bmatrix}\boldsymbol{C}. \tag{28}$$

It can be seen that we have linearized the nonlinear problem through the reversible mapping (24). The linearized result (28) allows us to use various classical linear control allocation methods. Herein, we employ the pseudo inverse method. The pseudo inverse solution is the two-norm solution to the control allocation problem and can be formulated as follows [23]:

$$\begin{aligned} &\min_{\boldsymbol{\delta}} J' = \min_{\boldsymbol{\delta}} \frac{1}{2}\left(\boldsymbol{\delta}' + \boldsymbol{c}'\right)^T \boldsymbol{W}\left(\boldsymbol{\delta}' + \boldsymbol{c}'\right) \\ &s.t. \quad \boldsymbol{B}\boldsymbol{\delta}' = \boldsymbol{d}_{des} \end{aligned} \tag{29}$$

where $\boldsymbol{W}$ is a weighting matrix and $\boldsymbol{c}$ is an offset vector. The desired result is

$$\boldsymbol{\delta} = -\boldsymbol{c} + \boldsymbol{W}^{-1}\boldsymbol{B}^T\left(\boldsymbol{B}\boldsymbol{W}^{-1}\boldsymbol{B}^T\right)^{-1}\left(\boldsymbol{d}_{des} + \boldsymbol{B}\boldsymbol{c}\right). \tag{30}$$

From the above discussion, we know that pseudo inverse method focuses on the energy minimization of the 2-norm

in each control step.

Back to our study, we obtain the pseudo inverse of $\boldsymbol{K}$ according to (28) and (30):

$$\begin{aligned}\boldsymbol{K}^{\#} &= \boldsymbol{W}^{-1}\boldsymbol{K}^{T}\left(\boldsymbol{K}\boldsymbol{W}^{-1}\boldsymbol{K}^{T}\right)^{-1} \\ &= \boldsymbol{K}^{T}\left(\boldsymbol{K}\boldsymbol{K}^{T}\right)^{-1} \quad (\boldsymbol{W}=\boldsymbol{I})\end{aligned}$$

$$= \frac{1}{6}\begin{bmatrix} 2 & 0 & 0 & 0 & 0 & 0 \\ -\sqrt{3} & -1 & 0 & 0 & 0 & 2l^{-1} \\ -1 & \sqrt{3} & 0 & 0 & 0 & 0 \\ \sqrt{3} & -1 & 0 & 0 & 0 & 2l^{-1} \\ -1 & -\sqrt{3} & 0 & 0 & 0 & 0 \\ 0 & 2 & 0 & 0 & 0 & 2l^{-1} \\ 0 & 0 & -2 & 0 & 4l^{-1} & 0 \\ 0 & 0 & -2 & -2\sqrt{3}l^{-1} & -2l^{-1} & 0 \\ 0 & 0 & -2 & 2\sqrt{3}l^{-1} & -2l^{-1} & 0 \end{bmatrix}. \tag{31}$$

After obtaining the pseudo inverse matrix $\boldsymbol{K}^{\#}$, we take $\boldsymbol{C}=\boldsymbol{K}^{\#}\boldsymbol{U}$, so that we get F_i, α_i, β_i by using the inverse mapping $\boldsymbol{\tau}=\Theta^{-1}(\boldsymbol{C})$. With regard to the saturation of actuators, we add several saturation function terms in the simulation program. Furthermore, it can be solved by the redistributed pseudo inverse method in the future work.

C. Nonlinear Disturbance Observer

Next, we consider the original system with the lumped disturbances as follows:

$$\begin{aligned}\dot{\boldsymbol{x}} &= f(\boldsymbol{x}) + g(\boldsymbol{x})\boldsymbol{U} + \begin{bmatrix} O_{6\times 6} \\ I_{6\times 6}\end{bmatrix}\begin{bmatrix} d_1 & d_2 & \cdots & d_6\end{bmatrix}^{T} \\ &= f(\boldsymbol{x}) + g(\boldsymbol{x})\boldsymbol{U} + p(\boldsymbol{x})\boldsymbol{d}\end{aligned} \tag{32}$$

where $p(\boldsymbol{x}) = [p_1(\boldsymbol{x}), p_2(\boldsymbol{x}), \cdots, p_6(\boldsymbol{x})]$ and $\boldsymbol{d}$ is the disturbance vector.

Then, based on some assumptions described in [30], the effective NDOB is presented as follows: [30]

$$\begin{cases}\dot{\boldsymbol{z}}_d = -\ell(\boldsymbol{x})\left[p(\boldsymbol{x})\left(\lambda(\boldsymbol{x}) + \boldsymbol{z}_d\right) + f(\boldsymbol{x}) + g(\boldsymbol{x})\boldsymbol{U}\right] \\ \hat{\boldsymbol{d}} = \boldsymbol{z}_d + \lambda(\boldsymbol{x})\end{cases} \tag{33}$$

where $\hat{\boldsymbol{d}}$ and $\boldsymbol{z}_d$ are the estimated disturbance vector and the internal state vector of the nonlinear observer, respectively. $\lambda(\boldsymbol{x})$ is a compensation gain matrix to be designed, and $\ell(\boldsymbol{x}) = \frac{\partial\lambda(\boldsymbol{x})}{\partial\boldsymbol{x}}$. Meanwhile, the proof of the observer stability can be found in [30]. In this study, these two matrices are chosen as follows:

$$\lambda(\boldsymbol{x}) = \left[\lambda_1 x_7, \lambda_2 x_8, \lambda_3 x_9, \lambda_4 x_{10}, \lambda_5 x_{11}, \lambda_6 x_{12}\right]^{T} \tag{34}$$
$$\lambda_i > 0 \qquad (i = 1, \cdots, 6)$$

$$\ell(\boldsymbol{x}) = \frac{\partial\lambda(\boldsymbol{x})}{\partial\boldsymbol{x}} = \left[O_{6\times 6}\ \operatorname{diag}\left(\lambda_1, \lambda_2, \cdots, \lambda_6\right)\right]. \tag{35}$$

According to the existing conclusion in [30], the feedback linearization controller can be expanded as follows:

$$\boldsymbol{U} = \Gamma(\boldsymbol{x})^{-1}\left[-b(\boldsymbol{x}) + \boldsymbol{V} + \Upsilon(\boldsymbol{x})\hat{\boldsymbol{d}}\right] \tag{36}$$

where $\Gamma(\boldsymbol{x})$, $b(\boldsymbol{x})$, and $\boldsymbol{V}$ are defined in (20). Meanwhile,

$$\Upsilon(\boldsymbol{x}) = \begin{bmatrix}\gamma_{11}(\boldsymbol{x}) & \cdots & \gamma_{16}(\boldsymbol{x}) \\ \vdots & \vdots & \vdots \\ \gamma_{61}(\boldsymbol{x}) & \cdots & \gamma_{66}(\boldsymbol{x})\end{bmatrix} \tag{37}$$

where

$$\begin{aligned}\gamma_{ij}(\boldsymbol{x}) &= -\sum_{k=0}^{r_i-2} c_{k+1}^{i}\mathscr{L}_{p_j}\mathscr{L}_f^{k}h_i - \mathscr{L}_{p_j}\mathscr{L}_f^{r_i-1}h_i \\ & i,j \in \{1,\cdots,6\}.\end{aligned} \tag{38}$$

In (38), it is known that $r_i = 2$ and $\mathscr{L}_{p_j}h_i = 0$, $i,j \in \{1,\cdots,6\}$ based on the (13) and (18); therefore:

$$\begin{aligned}\gamma_{ij}(\boldsymbol{x}) &= -\sum_{k=0}^{r_i-2} c_{k+1}^{i}\mathscr{L}_{p_j}\mathscr{L}_f^{k}h_i - \mathscr{L}_{p_j}\mathscr{L}_f^{r_i-1}h_i \\ &= -c_1^{i}\mathscr{L}_{p_j}h_i - \mathscr{L}_{p_j}\mathscr{L}_f h_i \\ &= -\mathscr{L}_{p_j}\mathscr{L}_f h_i \qquad i,j \in \{1,\cdots,6\}.\end{aligned} \tag{39}$$

According to (39), it is no longer necessary to adjust the parameters c_1^i, $i \in \{1,\cdots,6\}$. In summary, the final control law is obtained, i.e., (36).

IV. SIMULATION

A physical model of the proposed tri-rotor has been developed, but there are still some hardware debugging tasks that have not been completed. Therefore, our model parameters for the simulation experiments are based on those of the physical model, and the actual flight test has not been conducted. The detailed model parameters are shown as follows: the distance from centroid to rotor l is 0.413m, and the mass of UAV m is 1.5kg. The moment of inertia on the X, Y, Z axis I_x, I_y, I_z are 0.11586kgm^2, 0.11584kgm^2, 0.22980kgm^2, respectively. The disturbance observer coefficient $\lambda_i = 10.0 (i = 1,\cdots,6)$. The control coefficient $\sigma_{11}=6, \sigma_{12}=12, \sigma_{21}=6, \sigma_{22}=5, \sigma_{31}=2, \sigma_{32}=1$ and $\sigma_{i1}, \sigma_{i2} = 3.0 (i = 4,5,6)$. Three simulation experiments are conducted in this study to validate the proposed approach using MATLAB V9.5. To avoid the propeller hitting the shaft, we set $\alpha_{min} = -\frac{\pi}{2}$, $\alpha_{max} = \frac{\pi}{2}$, $\beta_{min} = -\frac{\pi}{2}$, $\beta_{max} = \frac{\pi}{2}$, which means $\alpha_i \in \left[-\frac{\pi}{2}, \frac{\pi}{2}\right]$ and $\beta_i \in \left[-\frac{\pi}{2}, \frac{\pi}{2}\right]$. Meanwhile, we set $F \in [0, 10]\, N$. The disturbance variables are set in order to verify the effectiveness of the NDOB as follows:

$$\begin{cases}\boldsymbol{d}_1 = 0 \qquad \boldsymbol{d}_2 = 0 \qquad \boldsymbol{d}_3 = 2\sin(\frac{\pi t}{20} - \frac{\pi}{6}) \\ \boldsymbol{d}_4 = 1.7 \quad \boldsymbol{d}_5 = 2.5 \quad \boldsymbol{d}_6 = 2\cos(\frac{\pi t}{20} - \frac{\pi}{6}) - 0.5.\end{cases} \tag{40}$$

In addition, Gaussian noise ($\mu = 0$, $\sigma^2 = 1$) is introduced into each simulation, increasing the reliability of the simulation results.

The simulation program is based on the dynamics model, control algorithm, and NDOB obtained in the previous

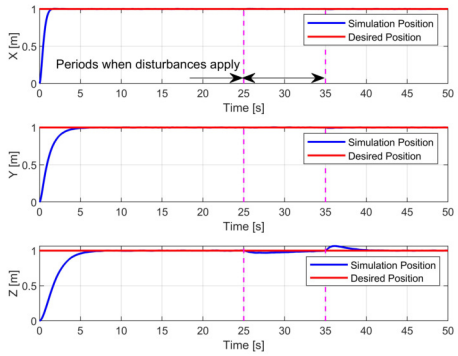

Fig. 4: Position of the UAV of Exp1: Hovering with changing attitude

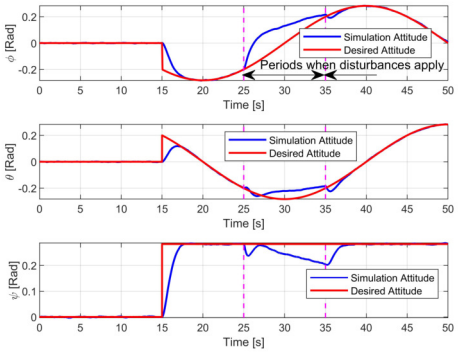

Fig. 5: Attitude of the UAV of Exp1: Hovering with changing attitude

discussion. The purpose of the simulation is to verify the high maneuverability of the UAV over the classical rotorcrafts and test the effectiveness of the control method we proposed.

1) Exp1: Hovering with Changing Attitude: Exp1 is intended to prove that our UAV can change the attitude angles according to the given rules we expect while hovering at a fixed point. In this simulation, the disturbance (40) applies at 25–35 s, and the UAV can hover at a point with changing attitude. The initial position and desired position are $(0,0,0)$m, $(1,1,1)$m, respectively. The initial attitude and desired attitude are $(0,0,0)$rad, $(0.2\sqrt{2}\cos 0.05\pi t, 0.2\sqrt{2}\sin 0.05\pi t, 0.2\sqrt{2})$rad, respectively. Herein, our proposed control method is applied in this simulation. Fig.4 and Fig.5 show the x, y, z coordinates and three attitude angles ϕ, θ, ψ, respectively.

The results of Exp1 proves the effectiveness of our proposed control method. The position and attitude of the UAV both converge to the desired target. Meanwhile, a classical rotorcraft cannot accomplish this task because when it changes its attitude during the hovering operation, it has a horizontal force component that changes its position.

2) Exp2: Zigzag with Horizontal Attitude by Applying NDOB or Not: Here, horizontal attitude means that roll, pitch, and yaw angle are all zero. The purpose of Exp2 is to prove that the effectiveness of NDOB. In this simulation, the disturbance (40) applies at 25–35 s, and the UAV can zigzag with horizontal attitude with or without NDOB to prove the effectiveness of the NDOB. The initial attitude and desired attitude are both $(0,0,0)$rad. The initial position is $(0,0,0)$m. We set the desired trajectory as follows:

$$\underbrace{\begin{cases} x_d = 1 \\ y_d = 1 \\ z_d = 1 \end{cases}}_{t\in(0,10s]} \Rightarrow \underbrace{\begin{cases} x_d = -\frac{2}{5}t + 5 \\ y_d = 1 \\ z_d = 1 \end{cases}}_{t\in(10,15s]} \Rightarrow \underbrace{\begin{cases} x_d = \frac{2}{5}t - 7 \\ y_d = -\frac{2}{5}t + 7 \\ z_d = 1 \end{cases}}_{t\in(15,20s]} \Rightarrow$$

$$\underbrace{\begin{cases} x_d = -\frac{2}{5}t + 9 \\ y_d = -1 \\ z_d = 1 \end{cases}}_{t\in(20,25s]} \Rightarrow \cdots \Rightarrow \underbrace{\begin{cases} x_d = \frac{2}{5}t - 19 \\ y_d = -\frac{2}{5}t + 13 \\ z_d = 1 \end{cases}}_{t\in(45,50s]} . \quad (41)$$

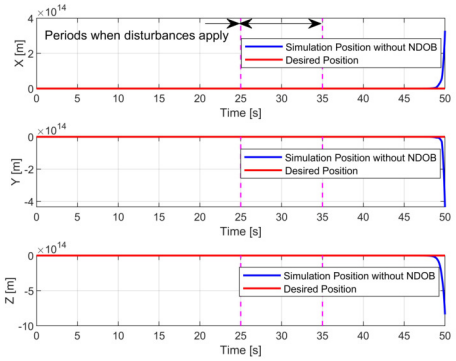

Fig. 6: Spatial trajectory of the UAV of Exp2: Zigzag with horizontal attitude (without applying NDOB)

Fig.6 presents the x, y, z coordinates of the fuselage without NDOB. It can be seen that the position of the UAV diverges under the influence of disturbance. Meanwhile, Fig.7 presents the fuselage spatial trajectory with NDOB, and Fig.8 and Fig.9 show the x, y, z coordinates and three attitude angles ϕ, θ, ψ with NDOB, respectively.

Again, this task cannot be conducted by the classical rotorcraft because it has to tilt its attitude when tracking a spatial trajectory. Fig.6 illustrates that the system may diverge under the influence of the disturbance without NDOB. Fig.7, Fig.8, and Fig.9 show that the disturbance can be effectively suppressed in the presence of NDOB. Exp2 proves that the NDOB we introduced can effectively compensate for the effects of disturbances and improve the robustness of the system.

3) Exp3: Spatial Ellipse with Horizontal Attitude by Applying Feedback Linearization or PID: Here, horizontal attitude means that roll, pitch, and yaw angle are all zero. The purpose of Exp3 is to compare our control method and

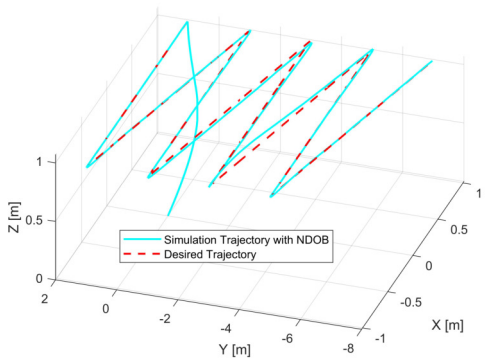

Fig. 7: Spatial trajectory of the UAV of Exp2: Zigzag with horizontal attitude (with applying NDOB)

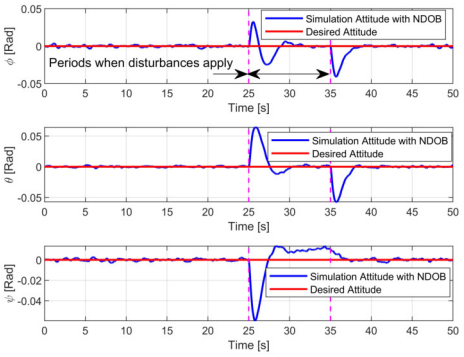

Fig. 9: Attitude of the UAV of Exp2: Zigzag with horizontal attitude (with applying NDOB)

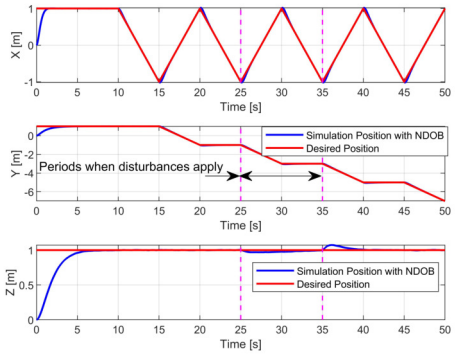

Fig. 8: Position of the UAV of Exp2: Zigzag with horizontal attitude (with applying NDOB)

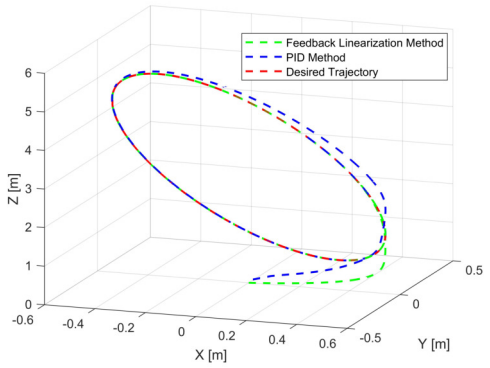

Fig. 10: Spatial trajectory of the UAV of Exp3: Spatial ellipse with horizontal attitude (Feedback Linearization vs PID)

classical PID method under the same task. In this simulation, the UAV can track the spatial ellipse with horizontal attitude by applying feedback linearization or PID to prove our control law are superior. The initial position and desired position are $(0,0,0)$m, $(0.5\cos 0.05\pi t, \quad 0.5\sin 0.05\pi t, \quad 3-2\cos 0.05\pi t)$m, respectively. The initial attitude and desired attitude are both $(0,0,0)$rad. Fig.10 presents the fuselage spatial trajectory. Fig.11 and Fig.12 show the x, y, z coordinates error in two control methods, and Fig.13 shows the three attitude angles ϕ, θ, ψ. Herein, we apply the classic PID method for comparison as follows:

$$\boldsymbol{U}_i = s_{i1}\left(x_{id} - x_i\right) + s_{i2}\int\left(x_{id} - x_i\right)dt + s_{i3}\left(\dot{x}_{id} - \dot{x}_i\right) \quad (i = 1, \cdots, 6) \tag{42}$$

where we have tried our best to tune these coefficients as follows: $s_{11} = s_{21} = 7500, s_{12} = s_{22} = 0, s_{13} = s_{23} = 1000, s_{31} = 20, s_{32} = 3, s_{33} = 20, s_{41} = s_{51} = 5.7, s_{42} = s_{52} = 1, s_{43} = s_{53} = 0.1, s_{61} = 7, s_{62} = 1.01, s_{63} = 0.15$.

All four figures show the comparison between our method and classical PID method. It can be seen from Fig.11 that the control effects of two method are similar in the X direction. The overshoot of our method is slightly smaller than the PID method in the Y direction, and the overshoot of the PID method is much larger than our method in the Z direction. Fig.12 considers the integrated error $E = \sqrt{e_x^2 + e_y^2 + e_z^2}$ of two methods. Obviously, our method integrated error is smaller than the PID method. Overall, Fig.10 visually illustrates the difference between the two methods. Meanwhile, the unit of the vertical axis in Fig.13 is 10^{-16}rad which is very small, so that both methods are ideal in attitude control.

In summary, the simulation results meet our expectations, and the position and attitude of the UAV can effectively and rapidly follow the track of the desired reference signal with a small error, thus validating the feedback linearization-based control method. The linear control law parameters σ_{i1}, σ_{i2} are appropriate because they have a good tradeoff between fluctuation and overshoot. NDOB significantly enhances the resistance to disturbance and the overall robustness of the system, thereby achieving the expected effect. These simulation results demonstrate the reliability of our hypotheses. Thus, we have laid the foundation and provided the theoretical basis for actual flight experiments in the future.

V. CONCLUSION

In summary, a novel over-actuated tri-rotor UAV system, its control method, and control allocator are introduced

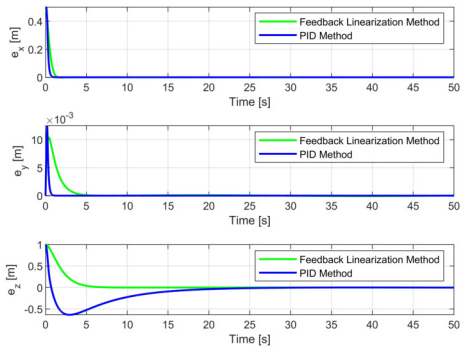

Fig. 11: Position error e_x, e_y, e_z of the UAV of Exp3: Spatial ellipse with horizontal attitude (Feedback Linearization vs PID)

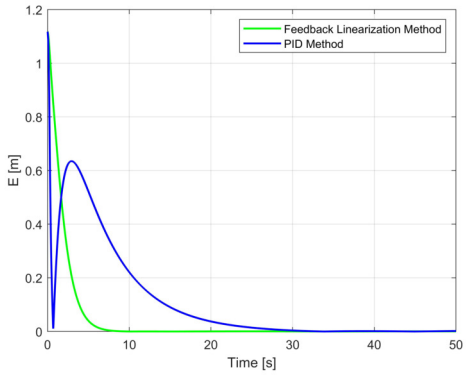

Fig. 12: Integrated position error $E = \sqrt{e_x^2 + e_y^2 + e_z^2}$ of the UAV of Exp3: Spatial ellipse with horizontal attitude (Feedback Linearization vs PID)

in this research field. The special structure of this UAV makes it more maneuverable while maintaining the attitude of the fuselage, providing wide application prospects, such as air–ground coordination. Meanwhile, actual flight tests will be conducted with a physical model of the proposed UAV and the UAV will be subsequently improved to have greater mobility in future. Moreover, the ability of the UAV to tolerate several actuators in the fuselage will also be investigated. Finally, a more efficient and robust control algorithm will be developed.

REFERENCES

[1] A. Das, K. Subbarao, and F. Lewis, "Dynamic inversion with zero-dynamics stabilisation for quadrotor control," *IET control theory & applications*, vol. 3, no. 3, pp. 303–314, 2009.

[2] Y. Yu, S. Yang, M. Wang, C. Li, and Z. Li, "High performance full attitude control of a quadrotor on so (3)," in *2015 IEEE International Conference on Robotics and Automation (ICRA)*. IEEE, 2015, pp. 1698–1703.

[3] M. A. Alsharif, Y. E. Arslantas, and M. S. Hölzel, "Advanced pid attitude control of a quadcopter using asynchronous android flight data," in *2017 International Conference on Unmanned Aircraft Systems (ICUAS)*. IEEE, 2017, pp. 1602–1607.

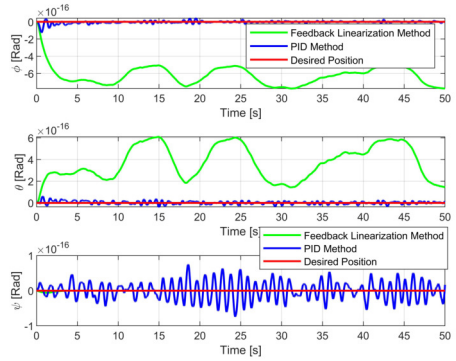

Fig. 13: Attitude of the UAV of Exp3: Spatial ellipse with horizontal attitude (Feedback Linearization vs PID)

[4] H. Kikkawa and K. Uchiyama, "Nonlinear flight control with an extended state observer for a fixed-wing uav," in *2017 International Conference on Unmanned Aircraft Systems (ICUAS)*. IEEE, 2017, pp. 1625–1630.

[5] G.-Y. Xia and Z.-H. Liu, "Quadrotor unmanned helicopter attitude control based on improved adrc," in *Proceedings of 2014 IEEE Chinese Guidance, Navigation and Control Conference*. IEEE, 2014, pp. 916–921.

[6] G. A. Garcia, S. Kashmiri, and D. Shukla, "Nonlinear control based on h-infinity theory for autonomous aerial vehicle," in *2017 International Conference on Unmanned Aircraft Systems (ICUAS)*. IEEE, 2017, pp. 336–345.

[7] D. A. Painter, N. Prabhakar, R. J. Prazenica, and M. J. Balas, "Trajectory-driven adaptive control of autonomous uavs with disturbance accommodation," in *AIAA Guidance, Navigation, and Control Conference*, 2017, p. 1523.

[8] C. Y. Son, H. Seo, T. Kim, and H. J. Kim, "Model predictive control of a multi-rotor with a suspended load for avoiding obstacles," in *2018 IEEE International Conference on Robotics and Automation (ICRA)*. IEEE, 2018, pp. 1–6.

[9] J. W. Langelaan and N. Roy, "Enabling new missions for robotic aircraft," *Science*, vol. 326, no. 5960, pp. 1642–1644, 2009.

[10] A. S. Saeed, A. B. Younes, S. Islam, J. Dias, L. Seneviratne, and G. Cai, "A review on the platform design, dynamic modeling and control of hybrid uavs," in *2015 International Conference on Unmanned Aircraft Systems (ICUAS)*. IEEE, 2015, pp. 806–815.

[11] E. J. Smeur, M. Bronz, and G. C. de Croon, "Incremental control and guidance of hybrid aircraft applied to a tailsitter unmanned air vehicle," *Journal of Guidance, Control, and Dynamics*, pp. 1–14, 2019.

[12] S. Swarnkar, H. Parwana, M. Kothari, and A. Abhishek, "Biplane-quadrotor tail-sitter uav: Flight dynamics and control," *Journal of Guidance, Control, and Dynamics*, vol. 41, no. 5, pp. 1049–1067, 2018.

[13] X. Lyu, H. Gu, J. Zhou, Z. Li, S. Shen, and F. Zhang, "A hierarchical control approach for a quadrotor tail-sitter vtol uav and experimental verification," in *2017 IEEE/RSJ International Conference on Intelligent Robots and Systems (IROS)*. IEEE, 2017, pp. 5135–5141.

[14] D. Brescianini and R. D'Andrea, "Design, modeling and control of an omni-directional aerial vehicle," in *2016 IEEE international conference on robotics and automation (ICRA)*. IEEE, 2016, pp. 3261–3266.

[15] C. J. Pratt and K. K. Leang, "Dynamic underactuated flying-walking (duck) robot," in *2016 IEEE International Conference on Robotics and Automation (ICRA)*. IEEE, 2016, pp. 3267–3274.

[16] S. Park, J. Her, J. Kim, and D. Lee, "Design, modeling and control of omni-directional aerial robot," in *2016 IEEE/RSJ International Conference on Intelligent Robots and Systems (IROS)*. IEEE, 2016, pp. 1570–1575.

[17] M. K. Mohamed and A. Lanzon, "Design and control of novel tri-rotor uav," in *Proceedings of 2012 UKACC International Conference on Control*. IEEE, 2012, pp. 304–309.

[18] P. Segui-Gasco, Y. Al-Rihani, H.-S. Shin, and A. Savvaris, "A novel

actuation concept for a multi rotor uav," *Journal of Intelligent & Robotic Systems*, vol. 74, no. 1-2, pp. 173–191, 2014.
[19] F. Şenkul and E. Altuğ, "Modeling and control of a novel tilt—roll rotor quadrotor uav," in *2013 International Conference on Unmanned Aircraft Systems (ICUAS)*. IEEE, 2013, pp. 1071–1076.
[20] ——, "Adaptive control of a tilt-roll rotor quadrotor uav," in *2014 International Conference on Unmanned Aircraft Systems (ICUAS)*. IEEE, 2014, pp. 1132–1137.
[21] M. Elfeky, M. Elshafei, A.-W. A. Saif, and M. F. Al-Malki, "Quadrotor helicopter with tilting rotors: Modeling and simulation," in *2013 World Congress on Computer and Information Technology (WCCIT)*. IEEE, 2013, pp. 1–5.
[22] H. Huang, "Control allocation of reaction control jets: quantization and stability," *Journal of Guidance, Control, and Dynamics*, vol. 38, no. 1, pp. 136–143, 2014.
[23] M. W. Oppenheimer, D. B. Doman, and M. A. Bolender, "Control allocation for over-actuated systems," in *2006 14th Mediterranean Conference on Control and Automation*. IEEE, 2006, pp. 1–6.
[24] T. A. Johansen, T. P. Fuglseth, P. Tøndel, and T. I. Fossen, "Optimal constrained control allocation in marine surface vessels with rudders," *Control Engineering Practice*, vol. 16, no. 4, pp. 457–464, 2008.
[25] T. A. Johansen, T. I. Fossen, and S. P. Berge, "Constrained nonlinear control allocation with singularity avoidance using sequential quadratic programming," *IEEE Transactions on Control Systems Technology*, vol. 12, no. 1, pp. 211–216, 2004.
[26] M. A. Bolender and D. B. Doman, "Nonlinear control allocation using piecewise linear functions," *Journal of Guidance, Control, and Dynamics*, vol. 27, no. 6, pp. 1017–1027, 2004.
[27] T. A. Johansen and T. I. Fossen, "Control allocation—a survey," *Automatica*, vol. 49, no. 5, pp. 1087–1103, 2013.
[28] S. Abdelmoeti and R. Carloni, "Robust control of uavs using the parameter space approach," in *2016 IEEE/RSJ International Conference on Intelligent Robots and Systems (IROS)*. IEEE, 2016, pp. 5632–5637.
[29] Z. Fang, Z. Zhi, L. Jun, and W. Jian, "Feedback linearization and continuous sliding mode control for a quadrotor uav," in *2008 27th Chinese Control Conference*. IEEE, 2008, pp. 349–353.
[30] J. Yang, S. Li, and W.-H. Chen, "Nonlinear disturbance observer-based control for multi-input multi-output nonlinear systems subject to mismatching condition," *International Journal of Control*, vol. 85, no. 8, pp. 1071–1082, 2012.